Journal of Sound and Vibration (1999) **226**(2), 237–251
Article No. jsvi.1999.2298, available online at http://www.idealibrary.com on IDEAL®

LOW-FREQUENCY SOUND TRANSMISSION IN DUCTS WITH PERMEABLE WALLS†

A. CUMMINGS AND R. KIRBY‡
School of Engineering, University of Hull, Hull HU6 7RX, England

(*Received* 27 *August* 1998, *and in final form* 25 *March* 1999)

A predictive model for sound propagation in tubes with permeable walls is presented. In this, acoustic coupling between the internal and external sound fields is taken into account by the use of an iterative procedure that involves finite-length "cells" of uniform properties in the tube and an appropriate external radiation model. The propagation model is verified by comparison to experimental data on a perforated metal tube and is applied to a practical type of permeable fabric tube. Good agreement between prediction and experiment is noted in the former case with predicted wall impedance values, and in the second case with "best fit" empirically derived wall impedance figures.

1. INTRODUCTION

Tubes with permeable walls are used in various applications, one of which is in the intake systems of internal combustion (IC) engines, where the tube is placed upstream of the air filter. A typical such tube might be made from wire-reinforced woven fabric. An understanding of sound propagation in permeable tubes is clearly desirable in the development of predictive design software for engine intake systems. The porous nature of the tube walls renders the internal wall impedance complex, so that an internally propagated sound field will be axially attenuated. But it can also introduce significant acoustic coupling between the interior and the exterior of the duct, and this feature distinguishes permeable-walled ducts from other types of soft-walled duct, in which internal/external acoustic coupling is usually minimal. For example, unlined ducts with impermeable but flexible walls radiate internal noise to the exterior *via* internally excited wall vibration (see, for example, the papers of Kuhn and Morfey [1] and Cummings [2]), but this tends to occur principally in narrow frequency bands around structural resonances of the walls. In unlined sheet metal ducts, coupling between wall vibration and the external sound field is usually weak and may be neglected (see the paper by Astley

†Some of the material in this paper was presented at the Inter-Noise 98 Conference in Christchurch, New Zealand, 16th–18th November 1998.

‡Now at the Department of Mechanical Engineering, Brunel University, Uxbridge UB8 3PH, U.K.

0022-460X/99/370237 + 15 $30.00/0

and Cummings [3]). In acoustically lined sheet metal ducts, the walls are usually sufficiently massive to inhibit internal/external sound transmission, though Cummings and Astley [4] have shown that this can be significant in the case of rectangular ducts with lightweight walls, where coupling between wall vibration and the internal sound field also needs to be taken into account.

In the present paper, a model for sound propagation in ducts with permeable but rigid walls is described. This is valid over the "low" frequency range in which the fundamental acoustic mode propagates with much lower attenuation than the higher order modes. The model incorporates the effects of both the duct-wall impedance and the external sound field, which is coupled—*via* acoustic motion through the wall—to the internal sound field. Mean air-flow effects are ignored, first because the mean flow Mach number in the tube would normally be small (at least in the context of IC engine intake systems), and secondly because any steady air flow through the tube walls would be so slow as to have little effect on the wall impedance. Numerical predictions of the axial sound pressure level distributions are compared to experimental data for both a perforated metal tube—used to verify the model—and a practical type of fabric tube, representative of those used in engine exhaust systems. The computed sound power flow components in the fabric tube are also discussed.

2. THEORY

The system depicted in Figure 1 will be considered here. A simple harmonic sound source of radian frequency ω radiates into the right-hand end of a circular-section permeable-walled tube of length L, located in an acoustic free field. This source could take the form of a plane-wave sound field incident from a rigid-walled pipe, or some other source type as long as the sound field that it generates consists principally of the fundamental mode of propagation. At the left-hand end of the permeable tube is a rigid-walled tube of the same internal diameter, in which only plane waves can propagate. This rigid tube is specified in terms of a plane-wave reflection coefficient at $x = 0$. Incident and reflected waves (denoted "i" and "r" respectively) are shown in Figure 1. It will be assumed that only the fundamental acoustic mode propagates at all points within the permeable pipe section. This assumption should be valid at sufficiently low frequencies, provided the axial attenuation rates of higher order modes are substantially higher than that of the fundamental mode. Because the permeable tube is of finite length, the external radiation load will not be constant along the length of the tube and, correspondingly, neither will the internal pipe wall impedance. This complicates the issue of modelling the internal sound field, and a straightforward uniform wall-impedance model for the whole tube cannot be used. Accordingly, a further assumption (see section 2.1) is that, although the internal pipe wall impedance—including the effects of the non-uniform external radiation load—may vary continuously along the axis of the pipe, a propagation model involving a piecewise uniform wall impedance is valid. This should be the case, provided appropriate matching conditions between the sound fields in the uniform-impedance sections are implemented, and that the length of each of these sections is

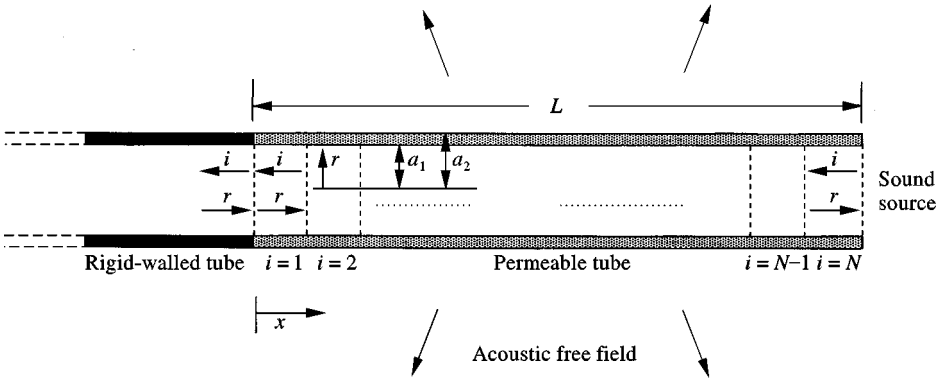

Figure 1. A permeable tube in an acoustic free field.

sufficiently small. Various authors have successfully used such "piecewise uniform" or "stepped" models in several contexts in duct acoustics (see for example the paper by Alfredson [5], concerning ducts of axially varying cross-sectional area).

2.1. THE ITERATIVE SOLUTION METHOD

Because a piecewise uniform wall impedance model is adopted here, it is convenient to divide the permeable tube axially into N "cells", all of equal length $2x_0$, numbered by the index i. The external sound pressure will be assumed here to be approximately constant over the length of each cell. And, if the duct walls are assumed to be locally reacting and permeable *but rigid* with a constant impedance ($\varsigma_w = \Delta p/u_n^{av}\rho c$, Δp being the acoustic pressure difference across the walls and u_n^{av} the average of the outer and inner outward normal particle velocity components), the analysis is simplified because the axial wavenumber and transverse mode function will be constant along the length of each cell. Continuity of acoustic force (i.e., sound pressure integrated over the cross-sectional area) and volume velocity for the fundamental mode, over the interfaces between cells, gives matching conditions which are employed in an iterative solution procedure that may be summarized as follows: (i) the incident and reflected wave amplitudes at $x = 0$ in the permeable tube are specified according to the reflection coefficient and the left-travelling plane wave amplitude in the rigid tube; (ii) the external sound pressures surrounding all cells are put equal to zero; (iii) the axial wavenumbers in the cells are found from the wall impedances and the external sound pressures, and incident and reflected sound pressure amplitudes are found for all cells, using the force and volume matching conditions between cells; (iv) the normal acoustic velocity through the pipe wall is found in each cell from the internal sound field from (iii) and the wall impedance; (v) the external sound pressure surrounding each cell is found from the mutual radiation impedances of the cells (see later).

The process from step (iii) to step (v) is repeated until convergence occurs. There may be an apparent contradiction in steps (ii)–(v) above at the first iteration, in that the assumed zero radiation load in step (ii) is incompatible with the idea of a normal

particle velocity through the pipe wall (step (iv)) and an associated external sound pressure field (step (v)). This is resolved when one notes that it is at step (iii) where the internal sound field is re-calculated by the use of the external sound field from the previous step. Not until the process has converged is the solution representative of reality.

2.2. THE INTERNAL SOUND FIELD

Within each cell, the sound pressures in the incident and reflected waves may be written as

$$p_i(r, x; t) = \mathrm{e}^{\mathrm{i}\omega t} P_i \mathrm{e}^{\mathrm{i}k_x x} \mathrm{J}_0(k_r r), \tag{1a}$$

$$p_r(r, x; t) = \mathrm{e}^{\mathrm{i}\omega t} P_r \mathrm{e}^{-\mathrm{i}k_x x} \mathrm{J}_0(k_r r), \tag{1b}$$

where P represents sound pressure amplitude, k_x, k_r are axial and radial wavenumbers for the fundamental mode, the radial factor in the sound fields is $\mathrm{J}_0(k_r r)$ and $\mathrm{J}_m(\,)$ is a Bessel function. Two adjacent cells are depicted in Figure 2. For convenience, they are labelled 1 and 2, and the conditions of acoustic force and volume velocity at section b lead to the relationships

$$P_{rb}^{(2)} + P_{ib}^{(2)} = [k_{r2}\mathrm{J}_1(k_{r1}a_1)/k_{r1}\mathrm{J}_1(k_{r2}a_1)](P_{ra}^{(1)}\mathrm{e}^{-i2k_{x1}x_0} + P_{ia}^{(1)}\mathrm{e}^{i2k_{x1}x_0}), \tag{2a}$$

$$P_{rb}^{(2)} - P_{ib}^{(2)} = [k_{x1}k_{r2}\mathrm{J}_1(k_{r1}a_1)/k_{x2}k_{r1}\mathrm{J}_1(k_{r2}a_1)](P_{ra}^{(1)}\mathrm{e}^{-i2k_{x1}x_0} - P_{ia}^{(1)}\mathrm{e}^{i2k_{x1}x_0}), \tag{2b}$$

between the incident and reflected sound pressure amplitudes in cell 2 at section b and those in cell 1 at section a.

The axial wavenumber k_x in each cell was found by solving the eigenequation

$$\varsigma_i \mathrm{J}_1(a_1\sqrt{k^2 - k_x^2}) - \mathrm{i}\frac{k}{\sqrt{k^2 - k_x^2}}\mathrm{J}_0(a_1\sqrt{k^2 - k_x^2}) = 0, \tag{3}$$

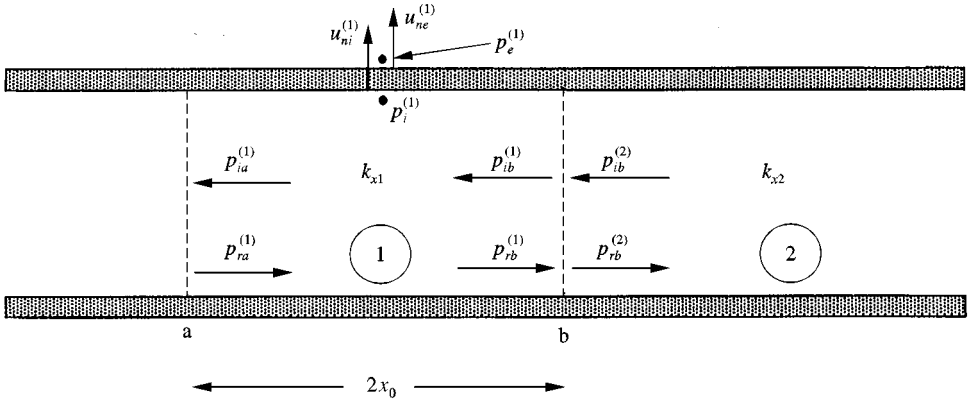

Figure 2. Two adjacent cells.

in which ς_i is the internal wall impedance, $\varsigma_i = p_i/u_{ni}\rho c$, ρ is the fluid density, $k = \omega/c$, c is the sound speed and p_i, u_{ni} are (respectively) the internal sound pressure at the tube wall halfway along the cell (say) and the corresponding outward normal particle velocity. (It is convenient to use the halfway point as the datum position, not for defining the impedance—where the axial position in the cell is immaterial—but in calculating the external sound pressure field, where the internal sound pressure at this position would be approximately representative of the average value in the cell.) Equation (3) was solved numerically by the use of Muller's method, and the starting value of k_x in this iterative process was found by inserting small argument approximations for $J_0(\ )$ and $J_1(\ )$ in equation (2) to yield (for the fundamental mode)

$$k_x \approx k\left[1 - \frac{\mathrm{i}}{ka_1(\varsigma_i/2 + \mathrm{i}ka_1/4)}\right]^{1/2}. \tag{4}$$

2.3. COUPLING BETWEEN INTERNAL AND EXTERNAL SOUND FIELDS

The internal wall impedance may be related to ς_w and the external sound pressure as follows. The outward normal particle velocities on the external and internal tube wall surfaces of (for example) cell 1 are denoted by $u_{ne}^{(1)}$, $u_{ni}^{(1)}$ and the corresponding pressures by $p_e^{(1)}$, $p_i^{(1)}$, all quantities again being defined at the axial centre of the cell. Then $\varsigma_i^{(1)}$ is given by

$$\varsigma_i^{(1)} = (1 + a_1/a_2)\varsigma_w/2 + p_e^{(1)}/u_{ni}^{(1)}\rho c, \tag{5a}$$

and one also has

$$u_{ne}^{(1)} = (a_1/a_2)p_i^{(1)}/\rho c\varsigma_i^{(1)} \tag{5b}$$

from continuity of volume velocity,

$$u_{ni}^{(1)}a_1 = u_{ne}^{(1)}a_2. \tag{5c}$$

Equation (5b) is also required in matching the internal and external sound fields via the wall impedance. Equivalent expressions hold, for course, for all cells.

2.3.1. *The internal sound field*

Equations (2a, b) may be used to relate P_i and P_r in cell 1 at $x = 0_+$ (which may be denoted P_{i0+} and P_{r0+}) to P_i and P_r in the rigid tube at $x = 0_-$ (which may be denoted P_{i0-} and P_{r0-}) as follows:

$$P_{r0+} = P_{i0-}\frac{k_{r1}a_1}{4J_1(k_{r1}a_1)}\left(R + 1 + \frac{R+1}{k_{x1}/k}\right), \tag{6a}$$

$$P_{i0+} = P_{i0-}\frac{k_{r1}a_1}{4J_1(k_{r1}a_1)}\left(R + 1 + \frac{R+1}{k_{x1}/k}\right), \tag{6b}$$

where $R = P_{r0-}/P_{i0-}$ and k_{r1}, k_{x1} are the radial and axial wavenumbers in cell 1.

In the experiments that are described later in this paper, a rigid plate was used to terminate the tube at $x = 0$ instead of the aforementioned anechoically terminated rigid-walled tube extension, because of the relative ease of fabrication. This corresponds to $R = 1$ in equations (6a, b), which yield $P_{r0+} = P_{i0+}$. This was used as the boundary condition at $x = 0$, and P_{r0+} was arbitrarily put equal to $1 + \mathrm{i}0$ pressure units.

2.3.2. *The external sound field*

The experiments involved a permeable tube with no axial extensions at either end, which may be approximated by a finite-length vibrating circular cylinder with rigid ends, for the purposes of computing the external sound field. In step (v) of the iteration procedure described in section 2.1, the mutual radiation impedance between two uniformly pulsating annular bands on the outer surface of the tube is required. Greenspon and Sherman [6] give theoretical results for uniformly pulsating curvilinear rectangular areas or "pistons" in an infinite rigid cylindrical baffle, but Cummings *et al.* [7] have shown numerically that the addition of rigid semi-infinite cylindrical baffles to the ends of a finite-length radiating cylinder make little difference to the radiation pattern. Accordingly, the results of reference [6] will be employed here. The effects of the finite impedance of the walls of the permeable tube will—perforce—be neglected in the present investigation. This should be a reasonable approximation provided the acoustic wavelength is significantly greater than the outer radius of the tube. For two pistons in a cylindrical baffle, the mutual radiation impedance is defined [6] as

$$Z_{ij} = (1/u_i) \iint_{s_j} p_i \, \mathrm{d}s_j, \tag{7}$$

u_i being the velocity of the ith piston (u_{ne} in the above nomenclature), p_i the sound pressure produced at the jth piston by the ith piston and s_j the area of the jth piston. If the cylinder radius is a, the axial dimensions of both pistons are $2x_0$, the axial separation of the pistons is x_{ij} and the pistons are fully annular, the result of reference [6] may be written

$$Z_{ij} = \mathrm{i}\ 8a\omega\rho \int_0^\infty \frac{H_0^{(2)}[a\sqrt{k^2 - \alpha^2}] \sin^2(\alpha x_0) \cos(\alpha x_{ij})}{\alpha^2 \sqrt{k^2 - \alpha^2}\, H_1^{(2)}[a\sqrt{k^2 - \alpha^2}]} \, \mathrm{d}\alpha \tag{8}$$

(where $H_m^{(2)}(\ )$ is a Hankel function), or alternatively

$$Z_{ij} = \mathrm{i}8a\omega\rho \left[\frac{1}{k^2} \int_0^\infty \frac{K_0(ka\alpha) \sin^2[kx_0\sqrt{\alpha^2 + 1}] \cos[kx_{ij}\sqrt{\alpha^2 + 1}]}{(\alpha^2 + 1)^{3/2} K_1(ka\alpha)} \, \mathrm{d}\alpha \right.$$

$$\left. - \frac{2}{k^2} \int_0^1 \left(B + \frac{\mathrm{i}4}{\pi ka\alpha} \right) \frac{\sin^2[kx_0\sqrt{1 - \alpha^2}] \cos[kx_{ij}\sqrt{1 - \alpha^2}]}{D(1 - \alpha^2)^{3/2}} \, \mathrm{d}\alpha, \right. \tag{9}$$

where

$$B = -2[\mathrm{J}_0(ka\alpha)\mathrm{J}_1(ka\alpha) + \mathrm{Y}_0(ka\alpha)\mathrm{Y}_1(ka\alpha)], \tag{10a}$$

$$D = 4\{[\mathrm{J}_1(ka\alpha)]^2 + [\mathrm{Y}_1(ka\alpha)]^2\}. \tag{10b}$$

$K_m(\ )$ is a modified Bessel function and $\mathrm{Y}_m(\ )$ is a Neumann function. The results of reference [6] have been corrected by a factor of $1/k^2$ and suitably modified for the "$+\,i$" notation used here. The sound pressure from the ith piston, space-averaged over s_j, is equal to $\langle p_i \rangle_{s_j} = u_i Z_{ij}/s_j$ where, of course, $s_j = 4\pi a x_0$. To determine the sound pressure at the jth piston, from all pistons *including* the jth, one simply has to find

$$\langle p_{tot} \rangle_{s_j} = (1/s_j) \sum_{i=1}^{N} u_i Z_{ij}. \tag{11}$$

Of course, since all the pistons have the same area in the present problem, $Z_{ij} = Z_{ji}$ (see equations (8, 9)), subject to the assumption of an infinite-impedance wall on the cylindrical baffle. And, furthermore, Z_{ij} only has to be computed N, rather than N^2, times since it is only the axial separation of the pistons that determines the mutual radiation impedance (for example, the mutual radiation impedance of the 5th and 12th pistons is the same as that of the 8th and 15th). The integrations in equation (9) were accomplished by the use of 12-point Gaussian quadrature, over an appropriate number of sub-intervals.

2.3.3. *The uncoupled solution*

For comparison purposes, the sound field inside the porous tube was found both with internal/external acoustic coupling (as outlined above) and without it. The uncoupled solution was found by putting $p_e = 0$ for all cells. Of course, no iteration was required beyond step (iii) in the process described in section 2.1, and the sound field in the duct was equivalent to that in a duct of constant wall impedance equal to $\varsigma_i = \varsigma_w(1 + a_1/a_2)/2$.

2.4. THE NET SOUND POWER LOSS IN THE POROUS TUBE

In the system considered, a portion (W_t) of the sound power W_i incident on the porous tube passes through the tube into the non-reflecting termination, a portion W_r is reflected back toward the source at the source end of the tube, and the balance (W_{inc}) is incident on the inner walls of the tube. Of this incident sound power, only a proportion W_{rad} is radiated to the exterior because of the dissipation in the walls of the tube. A control surface within the tube is depicted in Figure 3 and the components of the sound power flow are shown. These components may be expressed in terms of the field variables embodied in the solution scheme as follows:

$$W_i = \frac{\pi\,\mathrm{Re}(k_x^L)|P_i^L|^2}{\omega\rho} \int_0^{a_1} |\mathrm{J}_0(k_r^L r)|^2 r\,\mathrm{d}r, \qquad W_r = \frac{\pi\,\mathrm{Re}(k_x^L)|P_r^L|^2}{\omega\rho} \int_0^{a_1} |\mathrm{J}_0(k_r^L r)|^2 r\,\mathrm{d}r, \tag{12a, b}$$

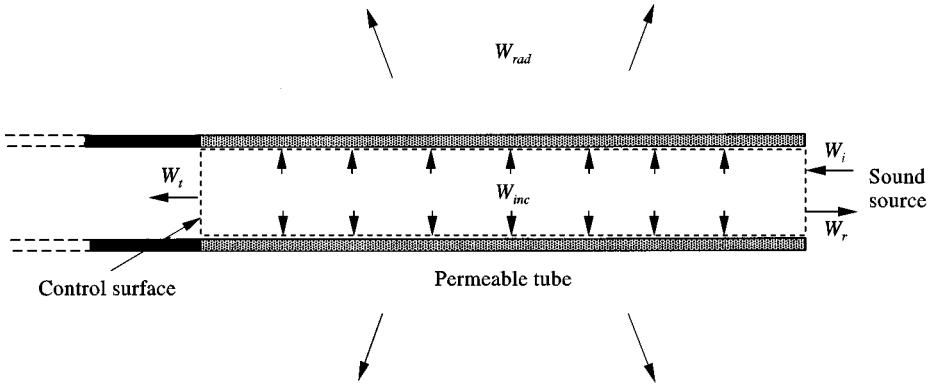

Figure 3. Sound power flow in the permeable tube.

$$W_t = \frac{\pi a_1^2 |P_{i0-}|^2}{2\rho c} = \frac{\pi a_1^2}{2\rho c} \quad (\text{since } |P_{i0-}| = 1), \tag{12c}$$

$$W_{rad} = 2\pi x_0 a_2 \sum_{i=1}^{N} \mathrm{Re}[p_e^{(i)}(u_e^{(i)})^*], \qquad W_{inc} = W_i - W_r - W_t, \tag{12d, e}$$

where the superscript L in equations (12a, b) denotes quantities in the Nth cell at $x = L$ and W_{rad} has been found by summing the radiated sound power contributions from all cells. Equation (12e) simply represents the acoustic power balance—at a steady state—in the control volume. The integration in equations (12a, b) were performed numerically by the use of 12-point Gaussian quadrature. In the tube walls, provided the wall impedance has a resistive component, there will be a net power dissipation

$$W_{diss} = W_{inc} - W_{rad} \tag{13}$$

which can be represented in decibel form in some convenient way. Here, we choose to define a "net sound power loss" ΔW as the logarithmic ratio between W_i and the remainder of this quantity, once the dissipated power has been subtracted. Therefore,

$$\Delta W = 10 \log\left(\frac{W_i}{W_i - W_{diss}}\right). \tag{14}$$

Clearly, for no dissipation, $\Delta W = 0$ whereas for $W_{diss} \to W_i$, $\Delta W \to \infty$.

3. EXPERIMENTS AND COMPARISON WITH THEORY

The apparatus shown in Figure 4 was used to measure the axial amplitude and phase distribution in a permeable tube, situated in a semi-anechoic environment. The transfer function between the microphone output and the loudspeaker input was measured at selected frequencies, and its modulus and phase were plotted versus

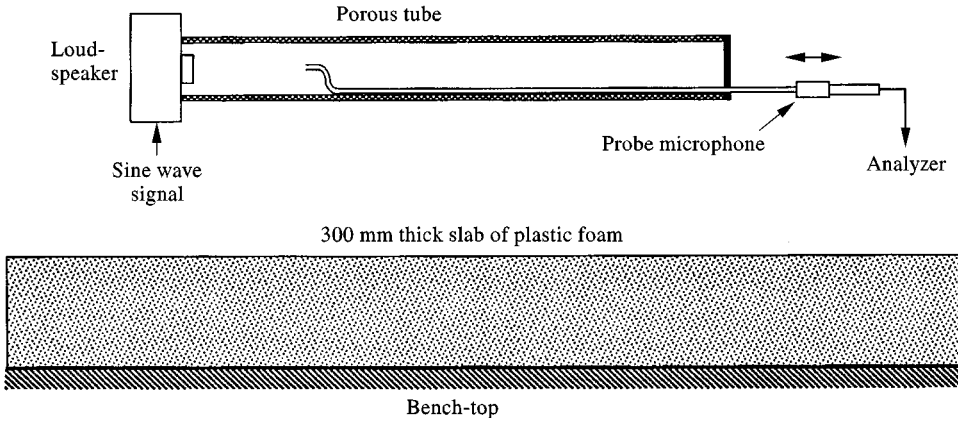

Figure 4. The experimental apparatus.

the axial distance from the rigid termination. Two tubes were used in the tests. The first was a circular aluminium tube with $a_1 = 28{\cdot}5$ mm, $a_2 = 31{\cdot}55$ mm and $L = 862$ mm (the effective length), perforated with 0·98 mm diameter holes to give an open area of 1·181%, and this was used to verify the theoretical model. The second was a flexible woven fabric tube (reinforced by a wire spiral) with circular section, of the type employed in IC engine inlet systems, and this was used as a practical example. It had $a_1 = 27{\cdot}5$ mm, $a_2 = 30{\cdot}5$ mm and $L = 776$ mm.

The theoretical results of Ingård and Ising [8], and of Hersh and Rogers [9], were used to predict the impedance of the holes in the aluminium tube—including both the viscous resistance and the reactance—and this impedance was divided by the fractional open area to give ς_w. The hole resistance expression of reference [8] is more appropriate to the present problem—where the orifice length is significantly greater than the diameter—than that of reference [9], and is given (in ρc units) by

$$\theta_h = \sqrt{8\omega\nu}(1 + t/d)/c, \tag{15a}$$

where ν is the fluid kinematic viscosity and t, d are the length and diameter of the perforate holes. The hole reactance expression of Hersh and Rogers [9] was used here in preference to that of reference [8] because it is felt to be more appropriate to the (actual) case in which an unsteady viscothermal boundary layer exists on the tube wall surrounding the orifice. This expression is (in ρc units)

$$\chi_h = k(t + d) + \sqrt{\omega\nu/2}/c \tag{15b}$$

and the total orifice impedance is given by $\varsigma_h = \theta_h + \mathrm{i}\chi_h$.

In the case of the fabric tube, difficulty was experienced in obtaining reproducible wall impedance data. Various types of test were carried out on flat samples of the wall material, and in all cases there was strong evidence of structural motion of the sample, which appeared to behave like a porous plate (also being orthotropic in its elastic properties because of the wire reinforcement). This, of course, meant that the

measured impedance represented not only permeability effects, but also structural effects dependent on the size, shape and boundary conditions of the sample. The steady flow resistance of the material was very high, and it is thought that this was partly responsible for the pronounced structural component of the impedance. Attempts were also made to measure the impedance of a cylindrical sample placed centrally in a cylindrical cavity, by the use of a two-microphone method. This too proved largely unsuccessful, mainly because of the difficulty in sealing the edges of the sample. The problems encountered in these measurements raise the question of whether structural motion is likely to be an important factor in the fabric tubes. This is an unresolved question, partly because of the complex nature of the tube-wall structure. It is thought, however, that structural motion would be much smaller in the case of a circular tube of the reinforced fabric material subjected to a circumferentially uniform forcing pressure than with a flat plate of the same material, subjected to a forcing pressure that was uniform in its plane. It is therefore tentatively suggested that wall motion is negligible in the case of the fabric tubes, except possible in cases where the flow resistance of the wall is extremely high.

Because of the difficulties in measuring the impedance of the reinforced fabric wall material, "best fit" effective impedance values have been used here in numerical predictions for the fabric tubes, obtained from comparisons to measured data. The accuracy of these is limited by the resolution of the data fitting, and the figures are taken to the nearest $0{\cdot}5\,\rho c$ units. Attempts to predict the wall impedance in a simple way from the steady flow resistance and mass per unit of the wall material in parallel proved to yield inaccurate results, and were abandoned.

3.1. MEASURED AND COMPUTED SOUND PRESSURE LEVEL DISTRIBUTION FOR THE ALUMINIUM AND FABRIC TUBES WITH RIGID TERMINATIONS

The measured and predicted axial sound pressure level (L_p) variations for the aluminium tube are shown in Figures 5(a–d) and those for the fabric tube are given in Figures 6(a–d). The L_p was measured on the centreline of the tube in all cases.

Predicted curves are shown, both with and without an external radiation load, i.e. with and without coupling between internal and external sound fields. The predicted axial dependence of L_p— with coupling—shown in Figures 5(a–d) agrees generally very well with the measured data. At 200 Hz, measurements for $x < 0{\cdot}352$ m suffered from a poor signal/noise ratio and are not shown, and the sharp dip in L_p at 500 Hz for $0{\cdot}3\text{ m} \leqslant x \leqslant 0{\cdot}35$ m is thought to be caused by an extraneous effect such as sound radiation from the loudspeaker casing. Otherwise, predicted and measured sound pressure patterns agree very closely, the maximum differences being only about 1–2 dB at 1 kHz. These small discrepancies may be attributed to imperfect prediction of the wall impedance at this relatively high frequency. Some evidence of instability in the iterative solution method was found for this tube in the mid-frequency range—particularly at 500 Hz—but this was minimized by avoiding the use of an excessive number of cells ($N = 20$ proved to be about optimum in the present case). The instability is partly a result of the relative transparency of the perforated aluminium tube to sound, and in more practical

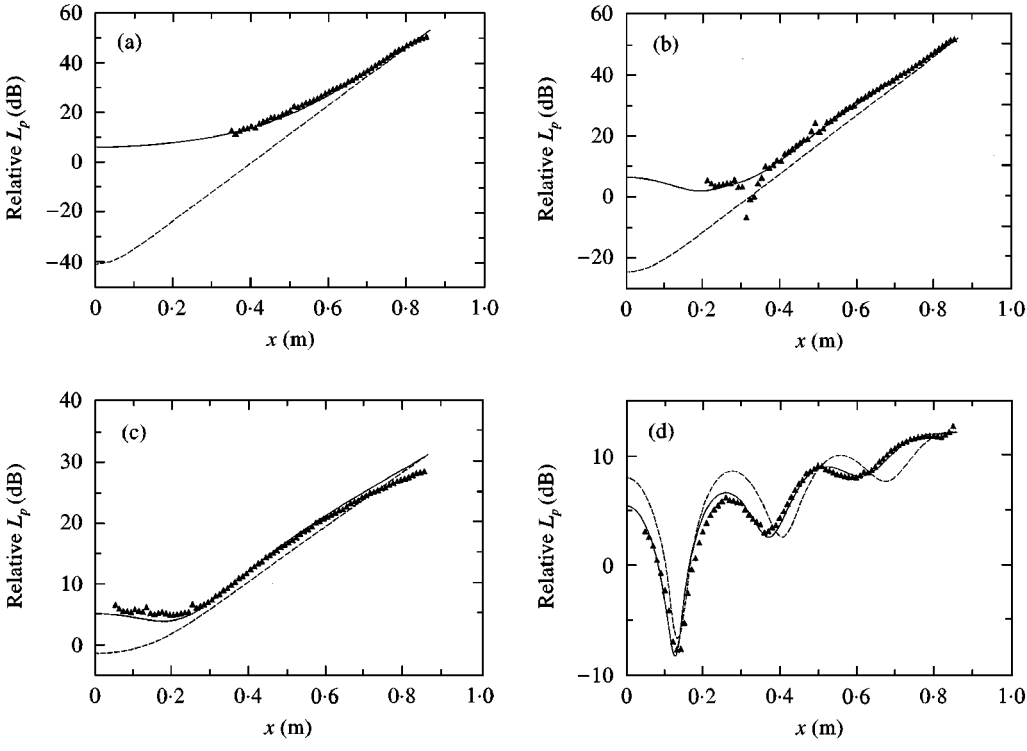

Figure 5. Axial variation in relative sound pressure level for the aluminium tube terminated by a rigid plate; ▲, measured data; ———, predicted (with radiation load); – – –, predicted (without radiation load). (a) 200 Hz, (b) 500 Hz, (c) 750 Hz, (d) 1 kHz.

cases where the wall impedance is higher—such as the fabric tube—instability was not a problem. It may be seen from Figures 5(a–d) that at the lower frequencies, the duct walls are relatively transparent to sound and a very large axial attenuation rate (roughly 90 dB/m at 500 Hz—for example—in the almost linear decay of the sound level over the first 0·5 m in front of the sound source) is apparent. At the higher frequencies however, the wall reactance (approximately $\propto \omega$) is high enough to inhibit sound radiation and cause a lower attenuation rate, together with a more prominent standing-wave pattern. This is particularly evident at 1 kHz. Very strong coupling between the internal and external sound fields is evident at the lower frequencies, since there is a dramatic difference between the predicted curves with and without a radiation load, particularly toward the rigid-tube termination. At 1 kHz, these differences lie more in the changes between the maximum and minimum L_p values, and in the positions of the minima.

The axial sound pressure level distribution in the aluminium tube has been computed from first principles, without the need for measurement of the wall impedance. One may therefore take the close correspondence between experiment and theory and the very pronounced effect of coupling between the internal and external sound fields as confirmation of the accuracy of the theoretical formulation and of the numerical data. Plots of the relative phase of the sound pressure are not

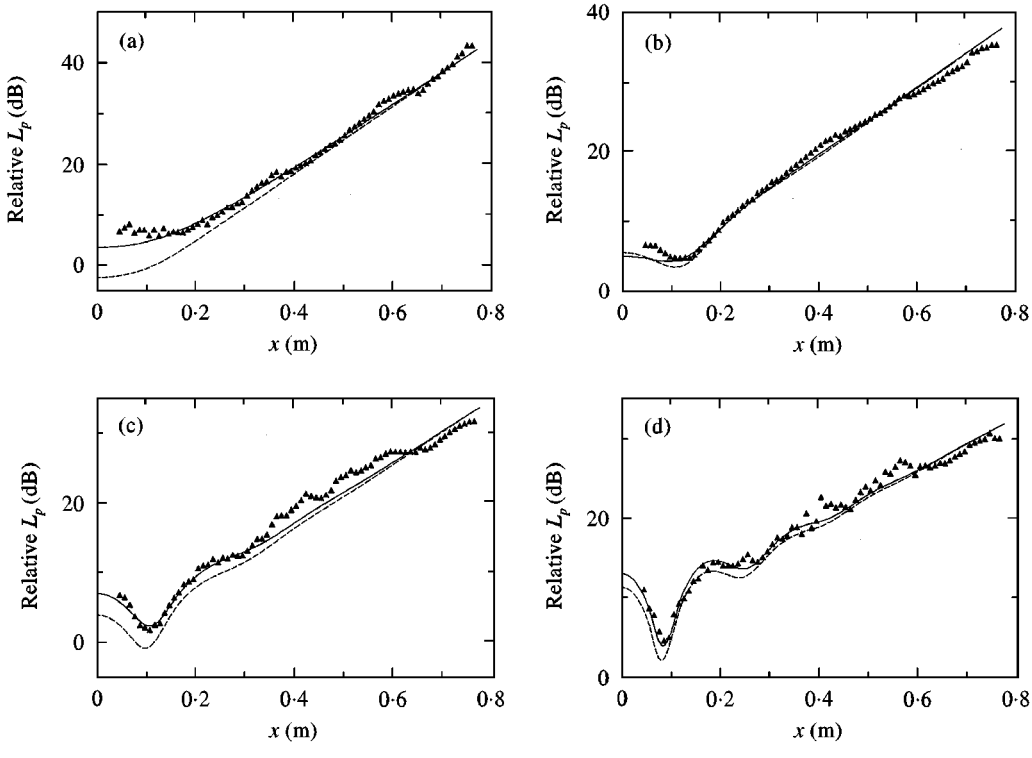

Figure 6. Axial variation in relative sound pressure level for the fabric tube terminated by a rigid plate; ▲, measured data; ———, predicted (with radiation load); – – –, predicted (without radiation load). (a) 250 Hz, (b) 500 Hz, (c) 750 Hz, (d) 1 kHz.

TABLE 1

"Best fit" wall impedance data for the fabric tube

f (Hz)	ς_w
250	3 + i2·5
500	6 + i0·5
750	7 + i1
1000	9·5 + i1

shown here since they contribute nothing additional to the discussion, but prediction—with coupling—and measurement generally agree well.

In the case of the fabric tube, "best-fit" wall-impedance data were obtained as outlined previously. The inferred values are given in Table 1. It can be seen that the real part of the impedance progressively increases from 3 to 9·5 as the frequency rises, while the imaginary part varies between 2·5 and 0·5. These impedance data were used in computing all the following predicted data on the fabric tube.

The predicted axial sound pressure level variation—with coupling—for the fabric tube shown in Figures 6(a–d) agrees well with the measured data, though the

latter show more scatter than those taken with the perforated aluminium tube, perhaps because of inhomogeneities in the wall impedance. As a result of the higher wall impedance in the case of this tube, there is less difference between the coupled and uncoupled predicted curves than there is with the perforated tube, though this difference can still be significant, particularly at 250 Hz. In the initially linear portion of the sound level decay, the axial attenuation rate is still large at the lower frequencies, being approximately 62 dB/m at 250 Hz and falling to about 35 dB/m at 1 kHz.

3.2. PREDICTED SOUND PRESSURE LEVEL DISTRIBUTION AND NET SOUND POWER LOSS FOR THE FABRIC TUBE WITH A NON-REFLECTING TERMINATION

It is of interest to predict the axial sound pressure level variation in the fabric tube with the rigid, non-reflecting, tube termination. Plots of these patterns are shown in Figures 7(a–d). As expected, acoustic reflection from the termination is fairly small, as indicated by the largely linear variation in L_p and minimal undulations in the curves. Perceptible—but small—undulations are evident at 1 kHz. In all curves, the axial impedance change at the termination brings about a change in slope of the L_p pattern at $x = 0$.

Perhaps of greater interest is the computed net sound power loss, and these data are shown in Table 2, together with values of W_i, W_r, W_t, W_{rad} and W_{diss}.

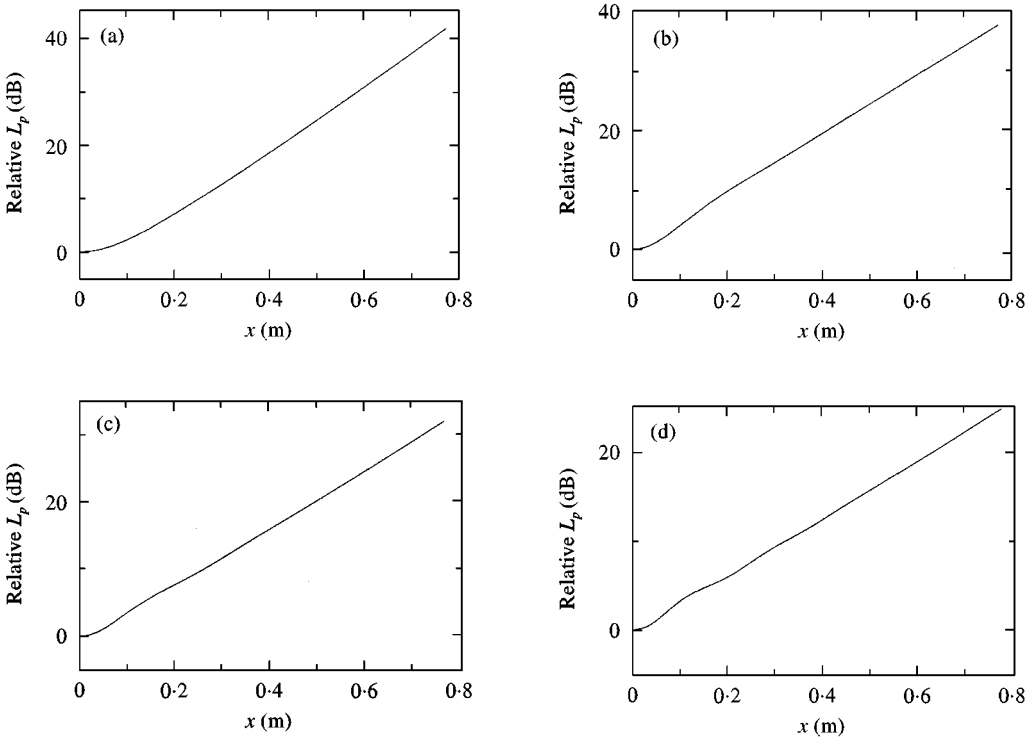

Figure 7. Axial variation in computed relative sound pressure level for the fabric tube terminated by a semi-infinite rigid walled tube. (a) 250 Hz, (b) 500 Hz, (c) 750 Hz, (d) 1 kHz.

TABLE 2

Sound power components and net sound power loss for the fabric tube with a non-reflecting termination

f (Hz)	W_i (Watt)	W_r (Watt)	W_t (Watt)	W_{rad} (Watt)	W_{diss} (Watt)	ΔW (dB)
250	$4{\cdot}12 \times 10^{-2}$	$1{\cdot}09 \times 10^{-6}$	$2{\cdot}88 \times 10^{-6}$	$7{\cdot}68 \times 10^{-4}$	$4{\cdot}04 \times 10^{-2}$	17·3
500	$1{\cdot}77 \times 10^{-2}$	$2{\cdot}95 \times 10^{-7}$	$2{\cdot}88 \times 10^{-6}$	$3{\cdot}93 \times 10^{-4}$	$1{\cdot}73 \times 10^{-2}$	16·5
750	$4{\cdot}48 \times 10^{-3}$	$5{\cdot}94 \times 10^{-8}$	$2{\cdot}88 \times 10^{-6}$	$1{\cdot}45 \times 10^{-4}$	$4{\cdot}33 \times 10^{-3}$	14·8
1000	$8{\cdot}45 \times 10^{-4}$	$5{\cdot}34 \times 10^{-9}$	$2{\cdot}88 \times 10^{-6}$	$2{\cdot}79 \times 10^{-5}$	$8{\cdot}14 \times 10^{-4}$	14·4

A surprisingly large sound power loss is apparent, and this is greater at the lower frequencies. Clearly, the fabric tube not only splits the incident sound power flow into reflected, transmitted and radiated components, but also brings about a substantial net dissipation. The figures for W_{diss} are, in all cases, not far short of the W_i values, so by far the greater proportion of the incident sound power is actually dissipated in the walls. An internal "transmission loss" (not including the radiated or dissipated sound power) could be defined as $10 \log(W_i/W_t)$, and one may see from the above figures that this falls from 41·6 dB at 250 Hz to 24·7 dB at 1 kHz.

4. CONCLUSIONS

The theoretical model for the internal and external sound fields in a tube with rigid porous walls, and in particular the coupling between the two, yields accurate results for the internal sound field in a perforated tube with easily predictable wall impedance. As previously mentioned, the iterative solution method can exhibit a degree of instability when the wall impedance is low, but the effects of this can be reduced by the avoidance of an excessive number of cells. In the case of practical types of tube with higher wall impedance, such as the fabric tube investigated here, instability is unlikely to be significant. Predicted and measured internal sound fields in this fabric tube were in good agreement, albeit with the use of an empirically determined wall impedance. The effects of coupling between the internal and external sound fields in the fabric tube were significant—particularly at low frequencies—but less marked than in the case of the perforated tube. The net sound power loss in the fabric tube was quite substantial, and was at its highest at low frequencies. This—together with the other sound power data given in Table 2—suggests that with careful design, permeable-walled tubes could constitute useful noise control elements. The external radiation impedance could, in principle, be tailored to optimize the internal wall impedance such that the axial attenuation was at a maximum while W_{rad} was still kept to an acceptable level.

The piecewise uniform duct wall impedance model, together with the assumption of purely fundamental mode propagation in the duct, appeared to be justified

within the frequency range of the present investigation. It is however reasonable to assume that, at higher frequencies, higher order mode propagation might be of some significance. The external radiation model [6] employed here was evidently adequate for the present purpose, and it is worth noting that a much simpler point source model for the mutual radiation impedance proved inaccurate.

The present model should provide a satisfactory basis for the acoustic design of practical duct systems incorporating permeable tubes. It could be refined to account for complications of geometry and to include the effects of mean gas flow, should this prove to be necessary. Future investigation of the utility of permeable tubes as noise-control devices would be of considerable interest and clarification of the role of structural vibration of the tube walls would be useful.

ACKNOWLEDGMENT

The authors are indebted to M. Patrick Blanchin, of Westaflex Automobile, Roubiax, France, who arranged the supply of flexible fabric tubes for the experimental tests.

REFERENCES

1. G. F. Kuhn and C. L. Morfey 1976 *Journal of Sound and Vibration* **47**, 147–161. Transmission of low-frequency internal sound through pipe walls.
2. A. Cummings 1983 *Journal of Sound and Vibration* **90**, 193–209. Higher order mode acoustic transmission through the walls of rectangular ducts.
3. R. J. Astley and A. Cummings 1984 *Journal of Sound and Vibration* **92**, 387–409. A finite element scheme for acoustic transmission through the walls of rectangular ducts: comparison with experiment.
4. A. Cummings and R. J. Astley 1995 *Journal of Sound and Vibration* **179**, 617–646. The effects of flanking transmission on sound attenuation in lined ducts.
5. R. J. Alfredson 1972 *Journal of Sound and Vibration* **23**, 433–442. The propagation of sound in a circular duct of continuously varying cross-sectional area.
6. J. E. Greenspon and C. H. Sherman 1964 *Journal of the Acoustical Society of America* **36**, 149–153. Mutual-radiation impedance and nearfield pressure for pistons on a cylinder.
7. A. Cummings, I.-J. Chang and R. J. Astley 1984 *Journal of Sound and Vibration* **97**, 261–286. Sound transmission at low frequencies through the walls of distorted circular ducts.
8. U. Ingård and H. Ising 1967 *Journal of the Acoustical Society of America* **42**, 6–17. Acoustic non-linearity of an orifice.
9. A. S. Hersh and T. Rogers 1976 *National Aeronautics and Space Administration Contractor Report NASA CR-2682*. Fluid mechanical model of the acoustic impedance of small orifices.